

Fourier transform infrared evaluation of microscopic scarring in the cardiomyopathic heart: Effect of chronic AT₁ suppression

Kathleen M. Gough,^{a,*} David Zelinski,^a Richard Wiens,^a Margaret Rak,^a
and Ian M.C. Dixon^b

^a Department of Chemistry, University of Manitoba, Winnipeg, Canada R3T 2N2

^b Institute of Cardiovascular Sciences, St. Boniface General Hospital Research Centre, University of Manitoba,
351 Tache Avenue, Winnipeg, Canada R2H 2A6

Received 6 November 2002

Abstract

Our primary aim was to investigate the use of Fourier transform infrared (FTIR) spectromicroscopy as an accurate assay of cardiac extracellular matrix remodeling. Abnormal rearrangement or remodeling of the cardiac extracellular matrix is known to contribute to cardiac dysfunction. The microscopic multifocal necrosis and scarring are modulated by chronic AT₁ receptor blockade in experimental cardiomyopathy; thus, we also wished to rationalize the spectromicroscopic differences among control, untreated cardiomyopathic (CMP), and losartan-treated cardiomyopathic (LOS) hearts according to the pathogenesis of experimental cardiomyopathy. Male UM-X7.1 cardiomyopathic Syrian hamsters at early and late (65 and 200 days) stages of cardiomyopathy were subjected to 4-week losartan (15 mg/kg/day continuous infusion) treatment. Focal collagen microdomain distribution was confirmed spectroscopically by observation of the collagen IR fingerprint in the 1000–1800 cm⁻¹ region. Synchrotron FTIR spectromicroscopic map data were obtained from control (F1-β strain) hamsters, nontreated cardiomyopathic, and losartan-treated CMP animals and imaged with mapping software, according to intensity of collagen fingerprint. Compared to controls, untreated late-stage CMP myocardium was characterized by elevated levels of fibrillar collagens and this was partially normalized with a 4-week losartan treatment. FTIR spectromicroscopy revealed that elevated collagen expression in focal microdomains is present in late-stage cardiomyopathy, and 4-week AT₁ blockade is associated with attenuation of collagen absorption in these lesions.
© 2003 Elsevier Science (USA). All rights reserved.

Keywords: FTIR spectromicroscopy; Raman spectromicroscopy; Cardiac fibrosis; Heart failure; Cardiomyopathy; Scar

While vibrational spectroscopy is a mature technique [1], the application of vibrational spectromicroscopy (both IR and Raman) to biomedical problems is a new and rapidly growing field. There are many techniques for identifying molecules associated with disease, ranging from simple staining of tissue to highly specialized methods including NMR, X-ray crystallography, protein sequencing, and binding by specific receptor molecules. IR provides a different type of information: imaging of molecular and structural composition directly in the untreated, unfixed, and unstained whole tissue. Both qualitative and quantitative information

about chemical composition, functional groups, and conformation may be determined from these spectra.

The distinct vibrational spectrum of collagen is conferred by the preponderance of glycine and proline (or hydroxyproline) and the variety of unusual conformations, and has been used for decades in the study of conformational variation and fibrillar self-assembly in vitro [1–10]. Recently we evaluated changes in collagen deposition in the right and left ventricular tissue of cardiomyopathic (CMP)¹ and control (CON) myocardium with FTIR attenuated total reflectance (ATR) spectroscopy

¹ Abbreviations used: CMP, cardiomyopathic; CON, control; ATR, attenuated total reflectance; CHF, congestive heart failure; LOS, losartan-treated cardiomyopathic; LV left ventricle; NSLS, National Synchrotron Light Source; SRC, Synchrotron Radiation Center.

* Corresponding author. Fax: +204-474-7608.

E-mail address: kmgough@ms.umanitoba.ca (K.M. Gough).

[11]. The objective 100% classification of the normal and diseased heart tissue was achieved through linear discriminant analysis aided by genetic algorithm selection of spectroscopically diagnostic regions in the mid-IR region. With the ATR technique, data are collected from randomly sampled tissue (sample size ca. $2 \times 2 \times 2 \text{ mm}^3$). The feasibility of spectroscopic detection of spatially resolved collagen distribution has been demonstrated with a laboratory-based IR microscope [12]; however, the spatial resolution was limited by the low emittance of the laboratory instrument source.

Synchrotron IR spectromicroscopy is a powerful tool used here for the first time for in situ identification of collagen distribution in thin sections of untreated heart tissue. This technique combines the chemical specificity of IR analysis with the diffraction-limited spatial resolution of the infrared microscope. The infrared light from a synchrotron source (~ 1000 times more intense than a standard bench IR source) is passed through a microscope, permitting rapid acquisition of data from a $10 \times 10\text{-}\mu\text{m}$ area of an $8\text{-}\mu\text{m}$ -thick tissue section. Information about multiple components in the sampled volume can be obtained from a single spectrum, including collagen, lipid, DNA, and noncollagen tissue proteins. With the computer-controlled mapping stage, an image of the component distribution can be built up from across a large area, with a $10\text{-}\mu\text{m}$ spatial resolution. Apart from the easily recognizable spectral signature of collagen, spectral analysis permits tissue component analysis based on relationships between spectral signatures and protein conformation, as well as other components such as lipids, DNA, and sugars. We note here that development of commercial benchtop FTIR with microscope and focal array detectors offers another option for the acquisition of good quality data without recourse to synchrotron sources.

The cardiomyopathic Syrian hamster (UM-X7.1 strain) is a useful model of hereditary cardiomyopathy that is linked to a mutation of the δ -sarcoglycan gene [13] and mimics the gradual progression of congestive heart failure (CHF) in humans [14,15]. In cardiomyopathic hearts, extracellular collagen remodeling has been identified as replacement fibrosis for necrosed muscle [16]. Net accumulation of collagens contributes to the pathogenesis of heart failure in cardiomyopathy due to secondary changes in passive stretch and lusitropic function of the heart. Elevated late-stage collagen turnover in hearts of cardiomyopathic hamsters is modulated by AT_1 receptor activation [17]. Previous data indicate modest attenuation of total left ventricle (LV) collagen from cardiomyopathic animals in the presence of pharmacologic angiotensin suppression as determined by hydroxyproline content of whole ventricular preparations [18] using standard biochemical methodology. These findings were subject to sampling limitations insofar as total collagen concentration was provided as an average throughout the ventricle and the analysis of subtle, i.e., microscopic, focal changes

in extracellular matrix deposition was impossible. Furthermore, it is known that specific alterations in the mechanical properties of microscopic fibrous regions of CMP (elastic stiffness) may occur without detectable changes in global hydroxyproline content [19]. Thus the development of a sensitive, accurate assay for the determination of collagen deposition in microinfarcts in cardiomyopathic hearts is warranted.

As the pathogenesis of this experimental model of cardiomyopathic hearts involves focality of myocardial lesions including myocytolysis and induction of microinfarcts throughout the left and right ventricular myocardium, multifocal collagen deposition is a major contributor to net cardiac fibrosis in experimental cardiomyopathy [19,20]. We had undertaken the current study to specifically examine whether antifibrotic treatment is associated with reduced collagen deposition in the microinfarct domains. To accomplish this, we obtained IR data maps at the synchrotron FTIR microscopes located at NSLS (National Synchrotron Light Source, Brookhaven National Laboratories, Upton, NY) and SRC (Synchrotron Radiation Center, University of Wisconsin Madison, WI). Collagen was imaged with the mapping software to provide direct physico-chemical assessment of collagen distribution in visually normal and, if any, microinfarct regions of all samples. Spectral analysis of other components was conducted wherever possible.

Materials and methods

Experimental model

Breeding male and female UM-X7.1 strain cardiomyopathic hamsters were obtained from the laboratory of Dr. G. Jasmin of the Department of Pathology, University of Montreal, Canada. An F1- β strain of Syrian hamster obtained from Charles River served as age-matched controls in our experiments. The effect of AT_1 receptor blockade was carried out using 4-week losartan infusion in male UM-X7.1 CMP animals (LOS) of 65 and 200 days of age. Losartan (15 mg/kg/day) [21] or vehicle (saline, 0.9% NaCl) was administered by surgical implantation of an osmotic mini pump (Alzet Corporation, La Jolla, CA) to the anterior dorsal region of each animal and delivery was maintained for 28 days by pump implantation, beginning at either 37 or 172 days of age. In our hands, this dosage provides an appropriate level of AT_1 receptor blockade and this is reflected in significant improvements in the progression of cardiac dysfunction in cardiomyopathy using various biochemical parameters [18]. For comparative purposes, age-matched saline-infused F1- β Syrian hamsters were also employed in these studies. Animals were sacrificed by decapitation at either 65 or 200 days of age. These age groups represent distinct early and end stages of cardiomyopathy [17] and we have

observed that animals from this colony expressing cardiomyopathic phenotype may survive until 244 ± 20 (SE) days. All experimental protocols for animal studies were approved by an appointed Protocol Management Review Committee located at the University of Manitoba, Canada, following guidelines established by the Canadian Council for Animal Care in association with the Canadian Institutes for Health Research.

Tissue preparation

Hearts were removed at sacrifice and excess fat, great vessels, and atrial tissues were excised and discarded. Ventricular tissues were dipped in OCT compound (Immunocor Canada Inc.), frozen, and then stored in liquid nitrogen (-196°C). This procedure ensures sample stability and permits better tissue slicing, without contamination of the tissue [22]. Serial cryostat sections were collected on reflective-coated microscope slides (Low-e MirrIR, Kevley Technologies, Chesterland, OH) for spectroscopic analysis and on standard glass slides for staining (hematoxylin and eosin; trichrome). The MirrIR slides provide essentially equivalent reflectance characteristics to gold in the infrared, but are transparent in the visible, and may be subjected to staining procedures.

IR spectromicroscopic data collection

Regions were selected for IR spectromicroscopic mapping after visual inspection of tissue-positive regions apparent in the trichrome-stained serial slides. Spectra were recorded in reflectance mode on a Nicolet 860 FTIR with a Continuum microscope (NSLS), or a Nicolet Magna 500 equipped with a Nic-Plan microscope (SRC). The Nicolet OMNIC/Atlas software was used for all data acquisition and map analyses. Typically, 128 or 256 interferograms were collected for each pixel, coadded, and ratioed to a similar background scan recorded at a blank region of the slide. The maps were saved as $\log(1/R)$, 4 cm^{-1} resolution spectra, encompassing the mid-IR region from 4000 to 800 cm^{-1} . The pixel size provides diffraction-limited spectra, where the diffraction limit is the inverse of the exciting wavelength; for a typical $10 \times 10\ \mu\text{m}$ aperture, this limit is about 1000 cm^{-1} . Below this limit, the signal to noise ratio decreases. Each map is an array of pixels with individually recorded spectra; map areas ranged from 100 to $100,000\ \mu\text{m}^2$. A CCD image of the region sampled, including a superposition of the map outline, was recorded with every map.

Collagen reference spectra

A pure collagen sample was prepared by applying $30\ \mu\text{l}$ of a collagen suspension (Type I, from rat tail, 4 mg/ml in 0.02 M acetic acid) to the reflective surface of a MirrIR slide. The slide was placed in a desiccator at ambient

temperature and pressure to remove solvent. Under these conditions, the film will dry to form native collagen fibers with characteristic triple-helical structures [5,7–10]. A collagen reference spectrum was acquired from the sum of 2048 interferograms (both sample and background).

Raman spectromicroscopic data collection

Raman spectra were obtained with a Renishaw confocal Raman spectrometer, employing a near-IR excitation line (782 nm) and a $1\text{-}\mu\text{m}$ spot size for illumination. The exciting wavelength is shorter than those used in IR, and the spatial resolution is correspondingly smaller. The diffraction limit is well below the actual spot size used. The Raman effect is inherently weaker than the IR, by a factor of about 1000. In addition, the Raman signal scattered from soft tissue is much weaker than that scattered from solid crystals. A single spectrum could be acquired in 10–30 min; however scans of 8 h were taken to ensure good signal to noise level. Under these circumstances, no mapping was done. Individual spectra of tissue and of crystalline deposits were acquired.

Map profiles and data processing

Collagen

Maps showing collagen distribution were created by comparing each spectrum in a map to that of pure collagen, for the truncated ($1167\text{--}1355\text{ cm}^{-1}$), baseline-corrected portion of the spectrum where the collagen fingerprint may be identified consistently. Absolute quantitation is not possible, as this requires not only the signal intensity but also the exact sample thickness, which varies throughout any tissue section. Results are shown on a scale from 0% remodeling (normal tissue) to 100% remodeling (essentially pure collagen as ascertained by computed correlation with the reference sample).

The collagen amide I and amide II bands are distinct from those of normal tissue; however, there is too much overlap between the band types to reliably use this region for analysis (see Results). The amide III region was found to be far superior for comparison purposes. In some cases, the postprocessing of data is considered to be an acceptable solution to the problem of complex and overlapping bands in biological samples [7,9,10,12,22]. However these methods (“resolution enhancement” or Fourier self deconvolution, and second derivatization) alter the original data, distort bands, and introduce artifacts. While they enhance the visual appearance of the data, they cannot alter the true spectral resolution, which is set by the instrument functions at the time of data acquisition and the intrinsic natural linewidths of energy absorptions. The spectral bands are composed of millions of overlapping, nearly identical peaks that cannot be resolved at any experimental spectral

resolution setting. Therefore, we have chosen to work exclusively with the data as originally recorded.

Lipid

The CH stretching region (2700–3100 cm⁻¹) of the infrared spectrum may be used to estimate lipid levels in a sample. Saturated long-chain hydrocarbons produce two strong absorption bands denoted as the symmetric and asymmetric CH₂-stretching modes [23–25]. Again, these are complex bands, composed of many millions of superimposed, nearly identical absorptions that overlap to produce two very reproducible maxima, distinct from the pair associated with CH₃ stretching. We have used the peak ratio of the more intense pair (2926:2959 cm⁻¹) to map for CH₂: CH₃ ratio. These features are a reliable indicator of lipid content.

Reagents

Rat tail collagen type I was purchased from Upstate Biotechnology (Lake Placid, NY). This collagen matches the predominant form of collagen in the remodeled tissue. Losartan was a kind gift from Merck and Co., Inc. Hemotoxylin and eosin staining as well as Masson's trichrome staining of hamster heart sections were performed by the Pathology Department at the St. Boniface General Hospital, Winnipeg, Canada.

Results

Tissue characterization

General characteristics of UM-X7.1 cardiomyopathic and F1-β control animals

The cardiomyopathic phenotype in 200-day UM-X7.1 animals was assessed as previously described and animals displaying classic markers of cardiomyopathy were used [18,26]. LV mass in 200-day cardiomyopathic animals was modestly lower than that of age-matched F1-β controls; however, absolute CMP LV mass increased significantly from 65 to 200 days (65-day CMP vs 200-day CMP values: 0.22 ± 0.01 g vs 0.35 ± 0.01 g, *P* < 0.05). On the other hand, comparison of LV mass values from 65- and 200-day F1-β control groups (65 F1-β vs 200-day F1-β values: 0.38 ± 0.04 g vs 0.40 ± 0.01 g) revealed no significant differences; essentially these animals are at the adult stage at 65 days. Based on intragroup comparisons, we suggest that relative cardiac hypertrophy occurs in CMP animals with advancing age, that this trend is absent in F1-β controls, and that the magnitude of cardiac hypertrophy is comparable to previous results [17,18,27]. Incidence of hypertrophy as determined by calculation of heart/body weight ratio data was not carried out, as the mean body mass in CMP animals from both ages is significantly decreased

compared to control values, yielding anomalous estimations.

Morphology and histopathology of tissue sections

Preliminary histochemical staining of serially cut LV tissue slices (hemotoxylin and eosin; Masson's trichrome) was performed to provide visual reference for areas examined spectroscopically. Representative photomicrographs of untreated tissue on MirrIR slides and trichrome-stained tissue on glass slides are shown in Fig. 1 for CON, CMP, and LOS samples. Locations selected for spectroscopic mapping are indicated by yellow boxes. Trichrome-stained CON hearts appear normal, with only faint traces of collagen, uniformly distributed throughout the tissue. Collagen appears as blue-stained material; however, some blue-stained material is attributable to lipid deposits or to staining of nonmyocytes, i.e., fibroblasts in the cardiac interstitium. Both 200-day CMP and age-matched losartan-treated hearts show some necrosis and focal collagen deposition throughout the mid-myocardium. Untreated CMP and losartan-treated LV tissue slices on MirrIR slides show areas of tissue damage, accompanied by white crystalline deposits that are attributed to calcium hydroxyapatite.

Spectromicroscopic results

Overview

The present work is an extension of our previous studies [11,12,28]; the principal technical improvement in the IR spectra lies in the significant increase in spatial resolution made possible through the use of a synchrotron IR source. In addition, we have analyzed the CH-stretching vibrations in the 2700–3100 cm⁻¹ region, as well as the collagen and normal protein vibrations in the fingerprint region (1800–800 cm⁻¹), to produce both collagen and lipid distribution maps. All mapping has been performed with close reference to tissue detail, and to corresponding trichrome-stained serial slices. Finally, Raman spectra of cardiac tissue and of crystalline deposits have been recorded with spatial resolution of 1 μm.

To ensure that data were acceptable, all spectra in a map were viewed serially prior to map analysis. Occasional problems were noted: (i) some spectra were too noisy for analysis to be meaningful; this occurred on rare occasions when data acquisition was not paused during beam fill procedure. (ii) IR spectra of the salt crystals were generally unusable, due to poor reflectivity off the uneven crystal surface, scattering, and high absorbance. (See Raman spectra of crystals, Fig. 8, below.) (iii) Absorbance due to water vapor was apparent in a few spectra. In most cases, the presence of water did not interfere with the data analysis, as the line intensity is very weak in the amide III region. Pixels that could not be analyzed due to any of the above problems represented less than 1% of the total number of spectra acquired.

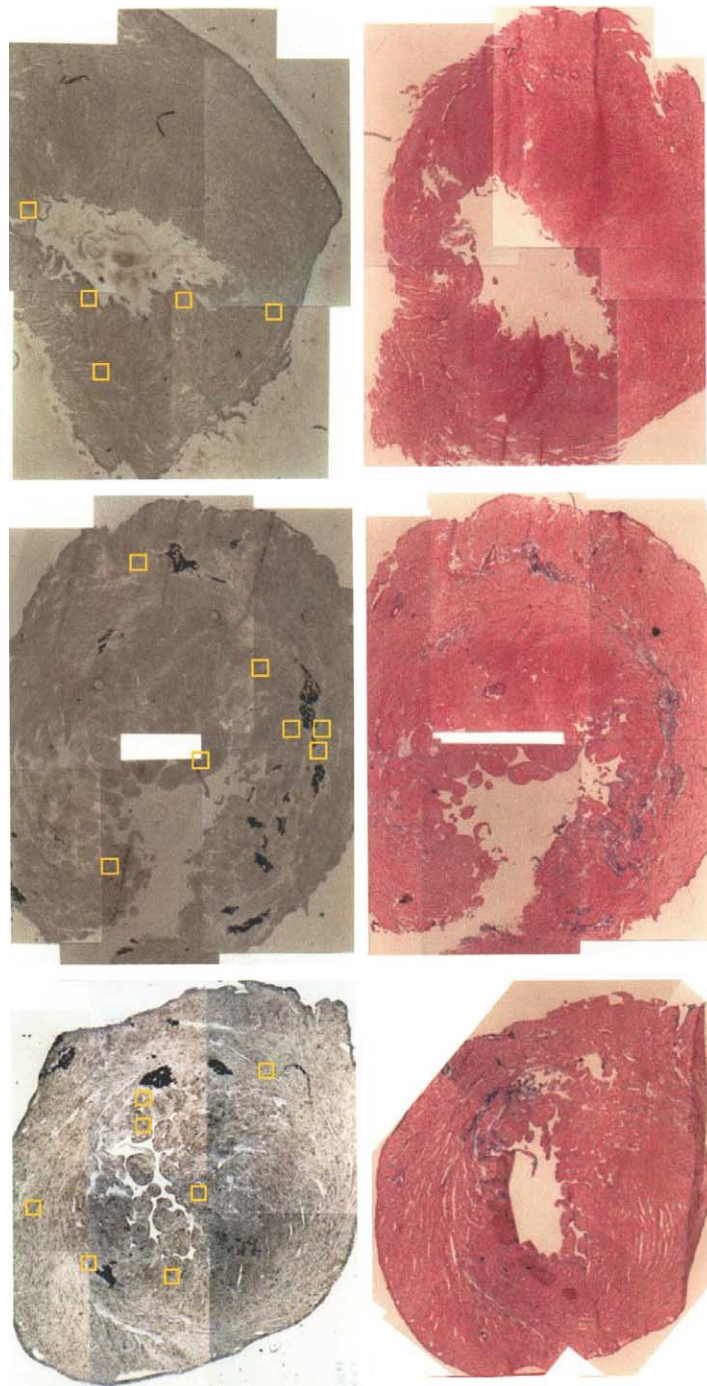


Fig. 1. Representative serial sections of CON, CMP, and LOS cardiac tissue on MirrIR substrate (left) and on glass with trichrome stain (right). Yellow boxes show locations of IR maps acquired on these tissues.

Collagen distribution maps

The IR absorption spectrum of pure collagen is well known, having been first published over 50 years ago, and studied extensively since [2–5]. Assignments for the major bands observed are based on the unusual abundance of glycine, proline and hydroxyproline, the corresponding absence of other amino acids, and on the triple helix conformation [7,9,10]. The “fingerprint region” of the spectrum ($1800\text{--}800\text{ cm}^{-1}$) of collagen type I is compared

to normal heart tissue and to remodeled tissue in Fig. 2. The tissue spectra have been extracted from maps recorded at $10 \times 10\text{-}\mu\text{m}$ pixel aperture. The collagen spectrum was recorded under the same experimental conditions, with the same aperture. The amide I band of collagen has a predominantly blue-shifted maximum at 1670 cm^{-1} and a lower energy shoulder at 1635 cm^{-1} , in marked contrast to the band maximum of 1656 cm^{-1} from the α -helical protein structure of normal tissue. It

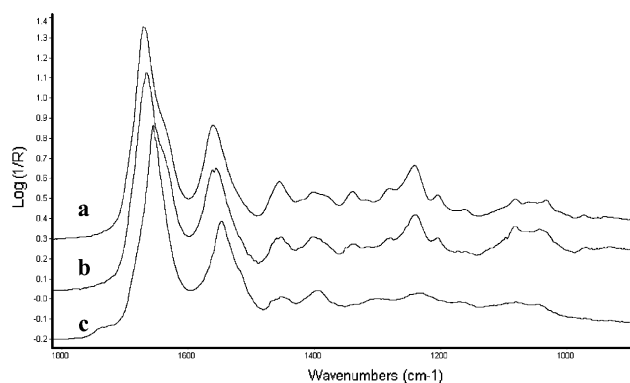


Fig. 2. Synchrotron IR spectra of (a) pure collagen (type I, rat tail), (b) remodeled cardiac tissue, and (c) normal cardiac tissue in the fingerprint region (1800–900 cm^{-1}).

has been postulated that the high-energy portion is due to the weakly hydrogen-bonded proline and hydroxyproline carbonyls, while the low-energy shoulder is due to the carbonyls of the glycine residues, which are strongly hydrogen-bonded to water [9,10]. The characteristic amide III bands of collagen [5,7,9,10] are observed at 1338, 1284, 1240, and 1204 cm^{-1} (mixed modes of amide III, CH_2 wagging, CH_3 deformation). Along with the unusual amide I and amide II profiles, these are associated with the triple helical structure. The region from 1000 to 1100 cm^{-1} is also distinct in collagen, with two small maxima at 1032 and 1082 cm^{-1} , generally ascribed to C–O vibrations of hydroxyl groups, either from hydroxyproline or from glycosidic side chains. Based on the similarity of the spectral profiles, the remodeled tissue in this example is classified as >90% collagen.

Collagen distribution in mapped areas of cardiac tissue samples was determined from the computed similarity between sample spectrum and that of pure collagen in the amide III range (1167–1355 cm^{-1}) for each

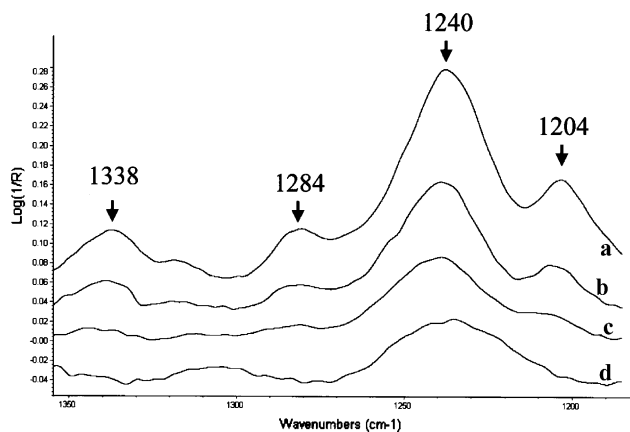


Fig. 3. Synchrotron IR spectra of cardiac tissue in the 1355–1167 cm^{-1} region, exhibiting (a) high (>90%), (b) medium (~60%), (c) low (~20%), and (d) negligible collagen remodeling, based on the intensity of the collagen bands at 1204, 1240, 1284, and 1338 cm^{-1} .

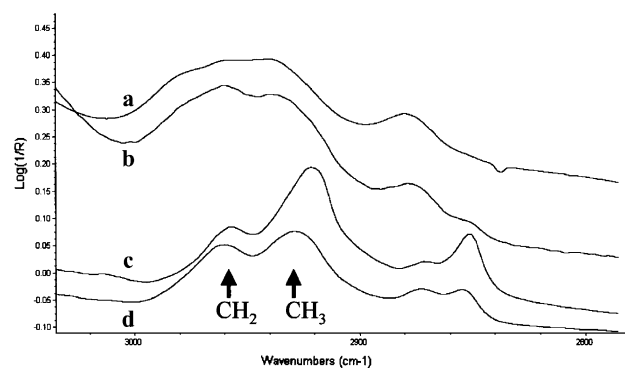


Fig. 4. IR spectra showing the CH stretch region (2700–3150 cm^{-1}) for (a) pure collagen, (b) remodeled cardiac tissue, and normal cardiac tissue with (c) typical lipid level and (d) maximum observed lipid level.

pixel in each map. These values are reported as percentage collagen based on the intensity of the signature bands. Representative spectra for these classifications are shown in Fig. 3. The phosphate band at 1238 cm^{-1} that is a feature of all normal tissue spectra is similar, though lower in intensity, to the amide III absorption of collagen but the characteristic collagen features are completely absent. While it is possible that there might be some very low levels of collagen in these spectra, our goal was to identify excessive collagen deposition.

Lipid distribution maps

The classic marker for lipid is the increased intensity of the CH_2 -stretching bands in the 2800–3000 cm^{-1} region, indicating the presence of the long hydrocarbon chain of fatty acid esters. In Fig. 4, the spectrum of pure collagen in the CH-stretch region is compared to normal tissue with and without high lipid content, and to remodeled CMP tissue. Average lipid content in normal tissue is low, resulting in a CH_2 : CH_3 peak ratio of about 1.4:1.0. In pockets with higher lipid content, the CH_2 symmetric and asymmetric stretch bands are greatly increased relative to the CH_3 bands, and the ratio exceeds 1.8:1.0. The collagen spectrum is different from that of normal tissue, reflecting the different amino acid components, and the absence of lipid. Note that, for collagen, the absence of lipids (typically indicative of cell membrane) results in a marked decrease in the CH_2 bands at 2926 and 2852 cm^{-1} . Instead, the CH of glycine and the slightly different CH_2 of the proline ring produce some bands in the same region, but the band maxima are shifted.

Lipid content in each spectrum (pixel) was evaluated from the ratio of the CH_2 to CH_3 -stretching vibration bands at 2852 and 2956 cm^{-1} , respectively. In nonfibrosed cardiac tissue, the relative lipid levels are readily mapped in this way. The band profile of pure collagen yields about equal intensity at these two frequencies; thus, the presence of collagen within a pixel cannot contribute to a false positive for lipid.

Map summary and images

The majority of maps were recorded from areas in the mid-myocardium, chosen to randomly represent the variation throughout the tissue, as indicated by the trichrome-stained serial slices.

Mapping of the 65-day hearts showed only normal collagen and lipid levels in both the CON and LOS myocardium. Some collagen was found in the region about the blood vessels in all three groups, see Figs. 5A and B. Regions of necrosis were identified only in the CMP hearts. In most cases, maps of these regions showed only necrosed tissue. Incipient remodeling was observed in some cases, as is demonstrated in Fig. 5C, a map in a necrosed region of 65-day CMP heart, where the collagen spectral signature reveals that remodeling had begun.

In Fig. 6, representative collagen distribution maps from each 200-day animal group (CON, CMP, and LOS) are contrasted to the lipid distribution maps created from the analysis of the CH-stretching region of the same spectral data files. The collagen content is described by the adjacent color-bar scale. For the lipid, the color scale corresponds to a range from low (red = CH₂:CH₃ ratio of <1.1) to high (blue >1.8). The mutual exclusion between lipid distribution (normal tissue) and focal collagen distribution (remodeled tissue) is evident in the paired lipid and collagen maps from the CMP sample. This confirms the absence of lipid in the replacement scar tissue of the infarct regions. Collagen distribution in CON tissue was uniformly low; strands of collagen were occasionally detected. Focal collagen was unmistakable in many of the mid-myocardium maps of CMP tissue and in some of the LOS tissue. Nonremodeled areas of CMP and LOS tissue closely resembled normal tissue in control hearts. The LOS samples also showed elevated amounts of focal collagen; however, there appeared to be less collagen than in the CMP tissues. Note that the white areas in the pair of LOS maps shown (Fig. 6 LOS) correspond to the location of crystalline deposits.

For simplicity, the total numbers of pixels showing collagen content in all maps, classified as low (<33%), medium (33–67%), and high (>67%), are summarized in Table 1. In the 65-day tissue, the collagen levels are essentially the same, at $2.3 \pm 0.9\%$ of all pixels recorded, in all three groups. The percentage collagen in the 200-day CON tissue is very low, consistent among the three cardiac samples from this group (2.7 ± 0.9), and comparable to that in the 65-day hearts. In all three 200-day CMP samples, it is significantly elevated (26.5 ± 10.6). The 200-day LOS set exhibits elevated collagen levels, but with large variability (11.1 ± 13.2), owing to particularly high collagen levels in heart 3.

IR and Raman spectra of salt crystal deposits

The untreated tissue slices contained salt deposits in the necrotic regions, while the presence of collagen is

confirmed in the corresponding region on the trichrome-stained serial slice (Fig. 7A). Much of the necrosis is obscured by the crystalline deposits in the unstained tissue; however, these have been washed away in the trichrome-stained sample. The underlying tissue is fragmented, suggestive of myocytolysis and granulosis, while much of the remaining intact area has been extensively remodeled. Under visible light, a small fold in the tissue may be seen across the top of the area to be mapped (Fig. 7B). Integration of the total band intensity for each pixel spectrum (Fig. 7C) illustrates the sensitivity of the detection method, as the slightly thicker tissue region absorbs more of the infrared light. Signal intensity in the processed false color map ranges from low (red) to high (blue). The crystalline regions also appear as points of greater absorbance; however, the IR spectra of the crystals are completely different from those of organic tissue, whether collagen or parenchyma. After spectral analysis to identify and map the collagen (Fig. 7D), they are easily differentiated from the other tissue (white indicates <10% match to collagen). The collagen is successfully identified in the remainder of the tissue, regardless of tissue thickness.

Vibrational Raman spectromicroscopy was used to confirm the identity of the crystalline deposit. The 1- μm diameter spot size allowed us to focus onto a single crystal facet. The IR spectra of the crystals were always very poor, due to the anomalous scattering of light off the uneven crystalline surface. However, the identity of the crystals was readily achieved through comparison of the Raman spectrum (Fig. 8A) with that of a standard spectrum of calcium hydroxyapatite (Fig. 8B). Evidence of collagen traces in the crystal is found in the presence of characteristic bands between 1200 and 1350 cm^{-1} (Fig. 8A, inset). Mineralization of heart tissue is a characteristic stage in the development of cardiomyopathy in the CMP hamsters and is present in many other diseases [29]; thus, the identity of the crystals is not surprising. The efficacy of the combined spectral analyses (IR and Raman) is noted.

Discussion

The UM-X7.1 strain of cardiomyopathic Syrian hamster provides a good model of hereditary dystrophic cardiomyopathy and CHF. It is characterized by progressive myocardial damage with subsequent dilatation of the ventricles, and is also associated with the hypertrophic phenotype [27,30]. The incidence of cardiomyopathy in this model is marked by the appearance of replacement fibrosis within the myocardium [17,31], and closely resembles the human form of this condition [32–34]. Excessive deposition of collagen and impaired compliance of the myocardium contribute to the occurrence of cardiac dysfunction [35]. Cardiac fibroblasts,

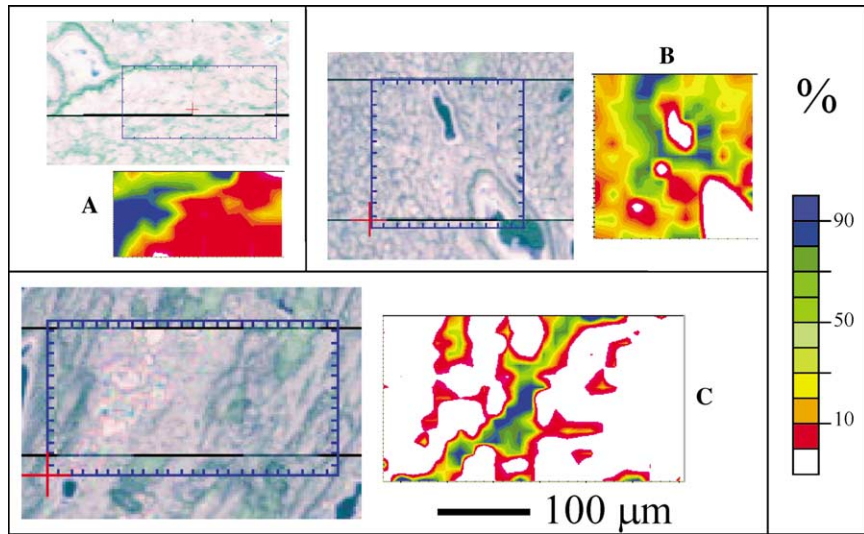


Fig. 5. FTIR imaging of collagen in 65-day cardiac tissue and video camera images of areas mapped. (A) Normal occurrence around blood vessels in CON tissue and (B) in CMP tissue. (C) Newly formed scar tissue detected as collagen in area of necrosis.

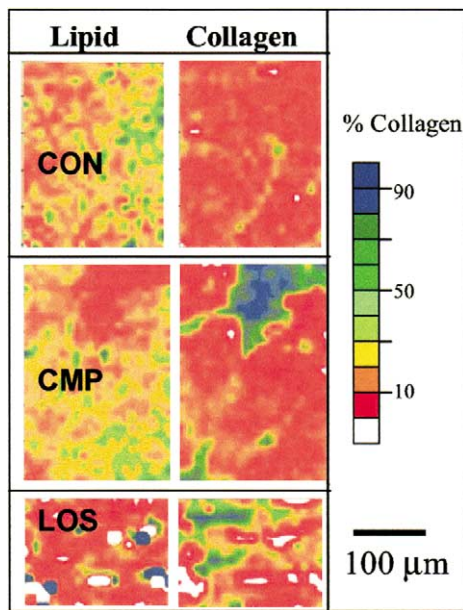


Fig. 6. Synchrotron IR maps of 200-day cardiac tissue from CON, CMP, and LOS samples, processed first for lipid (left) and then for collagen (right). Lipid content ranges from typical (red-yellow) to high (green-blue); see (c) and (d) in Fig. 4. Sidebar matches false-color scale to collagen content for collagen images. Note absence of lipid (red) in remodeled CMP and LOS tissue.

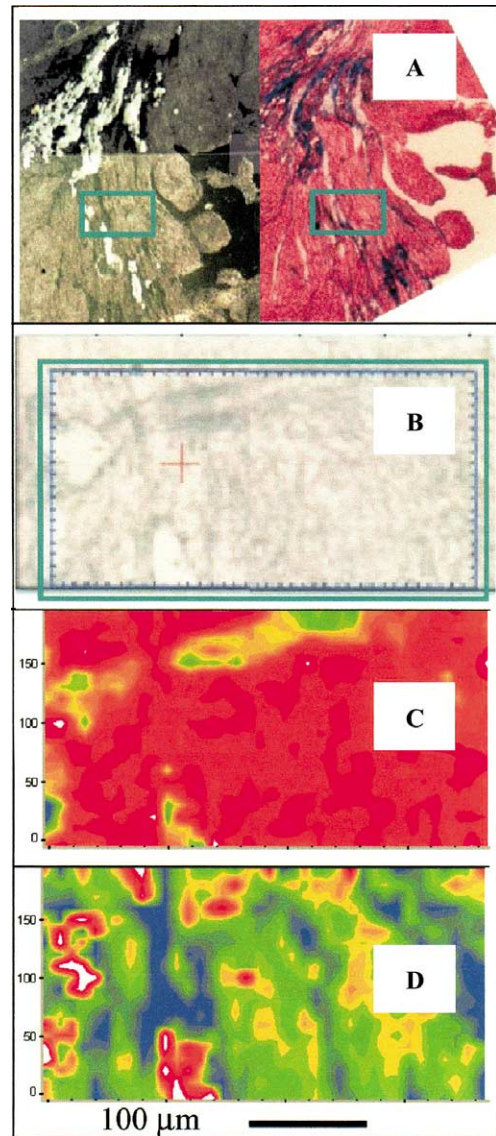


Fig. 7. (A) Serial tissue sections showing tissue with crystals on MirrIR substrate (left) and trichrome stain (right). (B) Videocamera image of area mapped. Green box outlines entire map area. (C) FTIR false-color map, processed to show total integrated intensity. Note region of tissue fold has greatest intensity (blue-green), as expected. (D) FTIR false-color map, processed for collagen levels. Note tissue is streaked with collagen (blue-green); tissue thickness does not interfere with collagen identification; microcrystalline deposits appear as white-red (spectrum is least like that of collagen).

Table 1
Collagen levels measured in FTIR maps of 65-day and 200-day hamster cardiac tissue

Sample	No. maps	No. pixels showing collagen			Sum	Total no. pixels mapped	% Collagen ^a
		Low	medium	High			
65-day cardiac tissue							
CON							
Heart 1	5	10	5	1	16	554	2.9
Heart 2	3	13	6	3	22	929	2.4
Heart 3	4	2	1	0	3	484	0.6
						<i>Mean</i>	2.0 ± 0.7
CMP							
Heart 1	9	3	2	2	7	249	2.8
Heart 2	7	21	5	2	28	1387	2.0
Heart 3	3	14	3	0	17	541	3.1
						<i>Mean</i>	2.6 ± 0.3
LOS							
Heart 1	4	3	1	0	4	150	2.7
Heart 2	4	2	2	1	5	154	3.2
Heart 3	5	2	0	0	2	170	1.2
						<i>Mean</i>	2.4 ± 0.6
200-day cardiac tissue							
CON							
Heart 1	7	21	17	9	47	1664	2.8
Heart 2	5	10	12	3	24	1452	1.7
Heart 3	5	12	0	0	12	346	3.5
						<i>Mean</i>	2.6 ± 0.5
CMP							
Heart 1	7	308	249	273	830	2225	37.3
Heart 2	6	153	97	74	323	2005	16.1
Heart 3	14	241	147	186	574	2198	26.1
						<i>Mean</i>	26.5 ± 6.1 ^b
LOS							
Heart 1	5	23	18	25	66	1285	5.1
Heart 2	7	18	14	8	40	1874	2.1
Heart 3	10	181	161	169	511	1943	26.3
						<i>Mean</i>	11.2 ± 7.6

^a All averaged values shown as ±SE.

^b $P < 0.01$ vs age-matched control values.

and especially cardiac myofibroblasts, are key players in fibroproliferative events associated with the major etiologies of heart disease [35,36] and express key genes supporting angiotensin expression [37]. The spectroscopic evaluation of collagen distribution (Table 1; Figs. 5–7) clearly shows the focal nature of remodeling in the CMP tissue. In the early stages (65-day cardiac tissue), there is much less evidence of cardiomyopathy. Both the CON and LOS tissues were completely free of visible lesions, suggesting cardioprotective effects of the losartan administration. As would be expected, some collagen was detected in the region surrounding blood vessels in all tissues; typical examples are shown in Figs. 5A and B. Each of the 65-day CMP tissues showed a few small infarct regions. Mapping of the necrosed tissue areas showed only some alterations in amide I consistent with necrosis. In one case, shown in Fig. 5C, a strand of collagen was found bridging the damaged cell region, indicating that scar tissue formation was underway.

In the 200-day CON samples, collagen is occasionally evident in the spectra; under the mapping profile it

appears as light streaks across otherwise normal tissue. As seen from the summary (Table 1), collagen-containing spectra represent only 2% of the total areas mapped in these CON samples. In comparison, the CMP maps showed collagen in high concentration, with some evidence of collagen in 27% of the spectra. The maps of LOS tissue had collagen in 12% of the pixels evaluated. The total numbers indicate a reduction in focal collagen in the losartan-treated hamsters; however, there is high variability within the group. As losartan treatment was introduced only 4 weeks prior to sacrifice, this indicates that there is only moderate, variable reduction of focal scarring upon treatment in late-stage cardiomyopathic hamsters.

Sampling is unavoidably subjective, as the total area mapped represents only about 1% of the total tissue surface. However, we consistently selected areas that were representative of the principal features of the tissues. In the case of the CON samples, the collagen was rare, and encountered randomly throughout the tissue. For the CMP and LOS samples, areas were selected to represent both normal and necrotic regions. The amount and extent

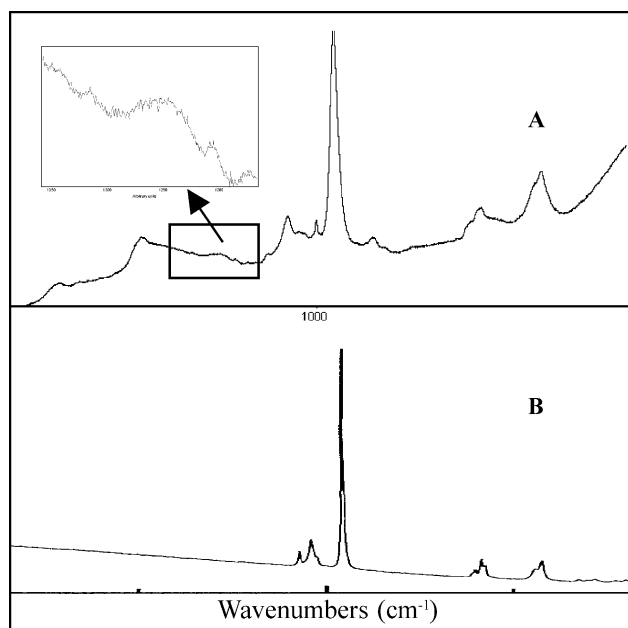


Fig. 8. Raman microspectroscopy of crystalline deposits in necrotic regions. (A) Raman spectrum of crystal (1- μm spot diameter). Insert: Expansion showing traces of collagen spectral signature at 1204, 1240, and 1284 cm^{-1} . (B) Raman spectrum of calcium hydroxyapatite (NIST).

of focal collagen present in the remodeled LOS tissue were generally less than those in the CMP tissue.

The IR spectroscopic detection of collagen could not be completely quantified, in that the exact tissue thickness at each pixel was not measurable. Upon comparison with the trichrome-stained tissues, particularly in the regions of heavy remodeling (for example, Fig. 7), we conclude that it provides a faithful image of the collagen present in the sample. There is an expected background level of collagen, thinly distributed throughout normal tissue, present in any sample. In our previous work, we found that, despite normalized collagen mRNA expression, only a modest decrease in total LV 4-hydroxyproline was observed in losartan-treated vs untreated CMP animals. However, entire left ventricles from each group were homogenized for the biochemical detection of total 4-hydroxyproline concentration, reflecting total cardiac collagen concentration. It was possible that, using this technique, the dilution of microfocal changes that occur within the fibrosed domains of local infarcts in CMP heart tissue was occurring. This suggestion is borne out by our current characterization of 4-week losartan-treated animals through spectromicroscopic mapping of intact tissue slices using high-intensity infrared light from a synchrotron beam source.

Lipid maps on CON, CMP, and LOS tissue reveal normal lipid levels in undamaged tissue at this spatial resolution. The remodeled regions show very little lipid, indicating that the normal cell structure has been completely replaced with collagen. Differences in relative amounts of lipid, normal tissue, and collagen result in

band shifts and intensity variations for all the vibrational modes of the CH, CH₂, and CH₃ in the fingerprint region, i.e., those modes commonly denoted as bending, wagging, rocking, scissoring [23–25]. It was incorrectly reported [28] that there was an increase in the CH₂ content relative to CH₃ content of fibrosed hamster cardiac tissue, on the basis of changes in the 1400–1500 cm^{-1} region of the spectrum. The authors had attributed the increased absorption at 1450 cm^{-1} to a CH₂-scissoring band. However, other studies [10] have assigned this band to ring-puckering vibrations of the prolines, which also absorb in this region. The CH-stretching region used in the present study, not examined by others [28], provides a more definitive measure of lipid content, as the CH band profiles are not contaminated or overlapped by other modes.

Four-week suppression of angiotensin AT₁ receptor function is associated with normalization of collagen deposition. Standard morphometric methods for collagen detection such as 4-hydroxyproline assessment of cardiac homogenate [38] from diseased (but not grossly infarcted) myocardium are designed for whole tissue sampling and lack that sensitivity required for multifocal microscopic cardiac scar assessment. This problem has confounded previous efforts to assess the quantal effects of angiotensin suppression on microinfarct remodeling in this experimental model. The IR mapping performed in this study provides a defined picture of the focal distribution of collagen in late-stage CMP and in losartan-treated CMP hamster heart tissue. Furthermore, FTIR is a sensitive screen for collagens and thus, in combination with relatively high spatial resolution, this spectroscopic method allows for a high degree of precision in the analysis of the microscopic scarring that is the hallmark of this experimental model of hereditary cardiomyopathy.

The FTIR spectromicroscopic map analyses are in agreement with our previous work, wherein we found modest dilute changes in the bulk cardiac matrix. More importantly, the spectroscopic analysis demonstrates that dramatic changes in collagen are found primarily in the focal microdomains. In the future, this technique may be transferred to benchtop IR microscopes for rapid evaluation of focal collagen deposition in this and other pathologies.

Acknowledgments

This study was supported by funding from the Canadian Institutes for Health Research and the Heart and Stroke Foundation of Manitoba (I.M.C.D.), as well as the Natural Sciences and Engineering Research Council and the University of Manitoba Research Development Fund (K.M.G.). I.M.C.D. is a CIHR group scientist. Raman spectral analysis was carried out at the Universite de Montreal, with the assistance of Dr. Tom Ellis. The SRC is funded by NSF (Award No. DMR-08442). The authors

are grateful to Dr. R. Julian (SRC) and Drs. L. Miller, L. Carr, and N. Marinkovic (NSLS) for assistance. We thank Mr. Stephen C. Jones and Mr. Justin Gawaziuk for their excellent technical assistance and input.

References

- [1] E.B. Wilson, J.C. Decius, P.C. Cross, *Molecular Vibrations: The Theory of Infrared and Raman Vibrational Spectra*, McGraw-Hill, New York, 1955.
- [2] R.D.B. Fraser, Infra-red microspectrometry with a 0.8 N.A. reflecting microscope, *Discuss. Faraday Soc.* 9 (1950) 378–383.
- [3] E.J. Ambrose, A. Elliot, Infrared spectra and structure of fibrous proteins, *Proc. R. Soc. London* 260 (1951) 206–219.
- [4] J.T. Randall, G.L. Brown, S. Fitton Jackson, F.C. Kelly, A.C.T. North, W.E. Seeds, G.T. Wilkinson, *Nature and Structure of Collagen*, Butterworth, London, 1953.
- [5] I.V. Yannas, Collagen and gelatin in the solid state, *J. Macromol. Sci.-Revs. Macromol. Chem. C* 7 (1972) 49–104.
- [6] W.H. Moore, S. Krimm, Vibrational analysis of peptides, polypeptides and proteins: polyglycine I, *Biopolymers* 15 (1976) 2439–2464.
- [7] R.J. Jakobsen, L.L. Brown, T.B. Hutson, D.J. Fink, A. Veis, Intermolecular interactions in collagen self-assembly as revealed by Fourier transform infrared spectroscopy, *Science* 220 (1983) 1290.
- [8] Y.A. Lazarev, B.A. Grishlovsky, T.B. Khromova, Amide I band of IR spectrum and structure of collagen and related peptides, *Biopolymers* 24 (1985) 1449–1478.
- [9] K.J. Payne, A. Veis, Fourier transform IR spectroscopy of collagen and gelatin solutions: deconvolution of the amide I band for conformational studies, *Biopolymers* 27 (1988) 1749–1760.
- [10] A. George, A. Veis, FTIRS in H₂O demonstrates that collagen monomers undergo a conformational transition prior to thermal self-assembly in vitro, *Biochemistry* 30 (1991) 2372–2377.
- [11] P.S. Bromberg, K.M. Gough, I.M.C. Dixon, Collagen remodeling in the extracellular matrix of the cardiomyopathic Syrian hamster heart as assessed by FTIR attenuated reflectance spectroscopy, *Can. J. Chem.* 77 (1999) 1843–1855.
- [12] K.Z. Liu, I.M.C. Dixon, H.H. Mantsch, Distribution of collagen deposition in cardiomyopathic hamster hearts determined by infrared microscopy, *Cardiovasc. Pathol.* 8 (1999) 41–47.
- [13] A. Sakamoto, K. Ono, M. Abe, G. Jasmin, T. Eki, Y. Murakami, T. Masaki, T. Toyo-oka, F. Hanaoka, Both hypertrophic and dilated cardiomyopathies are caused by mutation of the same gene, delta-sarcoglycan, in hamster: an animal model of disrupted dystrophin-associated glycoprotein complex, *Proc. Natl. Acad. Sci. USA* 94 (1997) 13873–13878.
- [14] B.M. Massie, N.B. Shah, Evolving trends in the epidemiologic factors of heart failure: rationale for preventive strategies and comprehensive disease management, *Am. Heart J.* 133 (1997) 703–712.
- [15] E. Bajusz, Hereditary cardiomyopathy: a new disease model, *Am. Heart J.* 77 (1969) 686–696.
- [16] K.T. Weber, C.G. Brilla, Pathological hypertrophy and cardiac interstitium. Fibrosis and renin-angiotensin-aldosterone system, *Circulation* 83 (1991) 1849–1865.
- [17] I.M.C. Dixon, H. Ju, N.L. Reid, T. Scammell-La Fleur, J.P. Werner, G. Jasmin, Cardiac collagen remodeling in the cardiomyopathic Syrian hamster and the effect of losartan, *J. Mol. Cell. Cardiol.* 29 (1997) 1837–1850.
- [18] I.M.C. Dixon, J. Hao, N.L. Reid, J.C. Roth, Effect of chronicreceptor blockade on cardiac Smad overexpression in hereditary cardiomyopathic hamsters, *Cardiovasc. Res.* 46 (2000) 286–297.
- [19] G. Davison, C.S. Hall, J.G. Miller, M. Scott, S.A. Wickline, Cellular mechanisms of captopril-induced matrix remodeling in Syrian hamster cardiomyopathy, *Circulation* 90 (1994) 1334–1342.
- [20] J.E. Strobeck, S.M. Factor, A. Bhan, M.J. Sole, C.C. Liew, F. Fein, E.H. Sonnenblick, Hereditary and acquired cardiomyopathies in experimental animals; mechanical, biochemical, and structural features, *Ann. N. Y. Acad. Sci.* 317 (1979) 59–88.
- [21] J.F. Smits, C. van Krimpen, R.G. Schoemaker, J.P. Cleutjens, M.J. Daemen, Angiotensin II receptor blockade after myocardial infarction in rats: effects on hemodynamics, myocardial DNA synthesis, and interstitial collagen content, *J. Cardiovasc. Pharmacol.* 20 (1992) 772–778.
- [22] M.G. Shim, B.C. Wilson, The effects of ex vivo handling procedures on the near-infrared Raman spectra of normal mammalian tissues, *Photochem. Photobiol.* 63 (1996) 662–671.
- [23] R.G. Snyder, J.H. Schachtschneider, Vibrational analysis of the *n*-paraffins I. Assignments of infrared bands in the spectra of C₃H₈ through *n*-C₁₉H₄₀, *Spectrochim. Acta* 19 (1963) 85–116.
- [24] J.H. Schachtschneider, R.G. Snyder, Vibrational analysis of the *n*-paraffins II. Normal coordinate calculations, *Spectrochim. Acta* 19 (1963) 117–168.
- [25] R.G. Snyder, Vibrational correlation splitting and chain packing for the crystalline *n*-alkanes, *J. Chem. Phys.* 71 (1979) 3229–3235.
- [26] V. Nigro, Y. Okazaki, A. Belsito, G. Piluso, Y. Matsuda, L. Politano, G. Nigro, C. Ventura, C. Abbondanza, A.M. Molinari, D. Acampora, M. Nishimura, Y. Hayashizaki, G.A. Puca, Identification of the Syrian hamster cardiomyopathy gene, *Hum. Mol. Genet.* 6 (1997) 601–607.
- [27] P. Di Nardo, R. Fiaccavento, A. Natali, M. Minieri, M. Sampaolesi, A. Fusco, C. Janmot, G. Cuda, A. Carbone, P. Rogliani, G. Peruzzi, Embryonic gene expression in nonoverloaded ventricles of hereditary hypertrophic cardiomyopathic hamsters, *Lab. Invest.* 77 (1997) 489–502.
- [28] K.-Z. Liu, M. Jackson, M.G. Sowa, H. Ju, I.M.C. Dixon, H.H. Mantsch, Modification of the extracellular matrix following myocardial infarction monitored by FTIR spectroscopy, *Biochim. Biophys. Acta* 1315 (1996) 73–77.
- [29] A. Carden, M.D. Morris, Application of vibrational spectroscopy to the study of mineralized tissues (review), *J. Biomed. Opt.* 5 (2000) 259–268.
- [30] H. Kawaguchi, M. Shoki, H. Sano, T. Kudo, H. Sawa, H. Okamoto, Y. Sakata, H. Yasuda, Phospholipid metabolism in cardiomyopathic hamster heart cells, *Circ. Res.* 69 (1991) 1015–1021.
- [31] E.W. Gertz, Cardiomyopathic Syrian hamster: a possible model of human disease, *Prog. Exp. Tumor Res.* 16 (1972) 242–260.
- [32] P. Di Nardo, M. Minieri, A. Carbone, N. Maggiano, R. Micheletti, G. Peruzzi, G. Tallarida, Myocardial expression of atrial natriuretic factor gene in early stages of hamster cardiomyopathy, *Mol. Cell. Biochem.* 125 (1993) 179–192.
- [33] J.E. Bishop, R. Greenbaum, D.G. Gibson, M. Yacoub, G.J. Laurent, Enhanced deposition of predominantly type I collagen in myocardial disease, *J. Mol. Cell. Cardiol.* 22 (1990) 1157–1165.
- [34] M. Wunsch, H.S. Sharma, T. Markert, S. Bernotat-Danielowski, R.J. Schott, P. Kremer, N. Bleese, W. Schaper, In situ localization of transforming growth factor beta 1 in porcine heart: enhanced expression after chronic coronary artery constriction, *J. Mol. Cell. Cardiol.* 23 (1991) 1051–1062.
- [35] K.T. Weber, Cardiac interstitium in health and disease: the fibrillar collagen network, *J. Am. Coll. Cardiol.* 13 (1989) 1637–1652.
- [36] D.J. Peterson, H. Ju, J. Hao, M. Panagia, D.C. Chapman, I.M. Dixon, Expression of Gi-2 alpha and Gs alpha in myofibroblasts localized to the infarct scar in heart failure due to myocardial infarction, *Cardiovasc. Res.* 41 (1999) 575–585.
- [37] G.W. Booz, K.M. Baker, Molecular signalling mechanisms controlling growth and function of cardiac fibroblasts, *Cardiovasc. Res.* 30 (1995) 537–543.
- [38] M. Chiariello, G. Ambrosio, M. Cappelli-Bigazzi, P. Perrone-Filardi, F. Brigante, C. Sifola, A biochemical method for the quantitation of myocardial scarring after experimental coronary artery occlusion, *J. Mol. Cell. Cardiol.* 18 (1986) 283–290.